Journal of Applied Physics

RESEARCH ARTICLE | JUNE 11 2024

Electron backscattering coefficients for Cr, Co, and Pd solids: A Monte Carlo simulation study

H. I. Imtiaz; M. S. S. Khan; A. Hussain ; S. F. Mao ; Y. B. Zou ; Z. J. Ding

Check for updates

J. Appl. Phys. 135, 225104 (2024)
https://doi.org/10.1063/5.0208968

View Online Export Citation

Articles You May Be Interested In

Uncertainty evaluation of Monte Carlo simulated line scan profiles of a critical dimension scanning electron microscope (CD-SEM)

J. Appl. Phys. (June 2023)

Comprehensive model of electron energy deposition

J. Vac. Sci. Technol. B (December 2002)

Comparison of MCNPX and GEANT4 to Predict the Contribution of Non-elastic Nuclear Interactions to Absorbed Dose in Water, PMMA and A150

AIP Conference Proceedings (August 2008)

06 December 2024 01:20:56

AIP Publishing

Journal of Applied Physics

Special Topics Open for Submissions

Learn More

AIP Publishing

Journal of Applied Physics ARTICLE pubs.aip.org/aip/jap

Electron backscattering coefficients for Cr, Co, and Pd solids: A Monte Carlo simulation study

Cite as: J. Appl. Phys. **135**, 225104 (2024); doi: 10.1063/5.0208968
Submitted: 18 March 2024 · Accepted: 27 May 2024 ·
Published Online: 11 June 2024

View Online Export Citation CrossMark

H. I. Imtiaz,[1] M. S. S. Khan,[2] A. Hussain,[3] S. F. Mao,[4,a)] Y. B. Zou,[5] and Z. J. Ding[1,6,a)]

AFFILIATIONS

[1]Department of Physics, University of Science and Technology of China, Hefei, Anhui 230026, People's Republic of China
[2]Key Laboratory of Materials Physics, Institute of Solid State Physics, Chinese Academy of Sciences, Hefei, Anhui 230031, People's Republic of China
[3]Institute of Advance Studies, Shenzhen University, Shenzhen, Guangdong 518060, People's Republic of China
[4]Department of Nuclear Science and Engineering, University of Science and Technology of China, Hefei, Anhui 230026, People's Republic of China
[5]School of Physics and Electronic Engineering, Xinjiang Normal University, Urumqi, Xinjiang 830054, China
[6]Hefei National Research Center for Physical Sciences at the Microscale, University of Science and Technology of China, Hefei, Anhui 230026, People's Republic of China

[a)]**Authors to whom correspondence should be addressed:** sfmao@ustc.edu.cn and zjding@ustc.edu.cn

06 December 2024 01:20:56

ABSTRACT

We have calculated electron backscattering coefficients, $\eta(E_p)$, at primary electron energies E_p of 0.1–100 keV for three elemental and intermediate atomic number solids, Cr, Co and Pd, with an up-to-date Monte Carlo simulation model. A relativistic dielectric functional approach is adopted for the calculation of the electron inelastic cross section, where several different datasets of optical energy loss function (ELF) are adopted. The calculated backscattering coefficient is found to be substantially affected by the ELF, where the influence can be seen to follow the *f*- and *ps*-sum rules and the resultant energy dependence of electron inelastic mean free path. To understand the uncertainties involved in a comparison with experimental data both the theoretical uncertainty due to the elastic cross-section model and the experimental systematic error for the contaminated surfaces are investigated. A total of 192 different scattering potentials are employed for the calculation of Mott's electron elastic cross section and this theoretical uncertainty is confirmed to be small. On the other hand, the simulation of contaminated Co and Pd surfaces with several carbonaceous atomic layers can well explain the experimental data. The present results indicate that accurate backscattering coefficient data should be either measured from fully cleaned surfaces or obtained from modern Monte Carlo theoretical calculations involving reliable optical constants data. With the recent progress in the accurate measurement of optical constants by reflection electron energy loss spectroscopy technique, constructing a reliable theoretical database of electron backscattering coefficients for clean surfaces of elemental solids is highly hopeful.

© 2024 Author(s). All article content, except where otherwise noted, is licensed under a Creative Commons Attribution-NonCommercial-NoDerivs 4.0 International (CC BY-NC-ND) license (https://creativecommons.org/licenses/by-nc-nd/4.0/). https://doi.org/10.1063/5.0208968

I. INTRODUCTION

The study of electron matter interaction is of great interest for many researchers due to the application of signals produced during this interaction in various techniques.[1–3] When an electron beam impinges on a solid target, the incident electrons will lose energy and change the direction of motion inside the solid. The interaction of electrons with a medium is, thus, described by the elastic scattering processes due to the collision with atomic nuclei and inelastic scattering processes due to the collision with electrons in the medium.[4] The inelastic scattering includes core electron excitation and ionization, interband transition, free electron excitation, and plasmon excitation. The majority of the emitted electrons from medium surface are secondary electrons and backscattered electrons, where the energies of secondary electrons are less than 50 eV and the backscattered electrons carry higher energies up to primary energy.[5,6] Secondary electrons are produced in a cascade process in

© Author(s) 2024

the medium and only those secondary electrons generated within the sub-nanometer thick layer of the surface can escape from the sample.[7] The secondary electron signals tend to be highly localized at the point of impact of the primary electron beam and are sensitive to the surface topography, making it possible to form a scanning electron microscopic (SEM) image of the sample surface. Backscattered electrons are those incident electrons reflected back from the target specimen and accompanied by a certain amount of energy loss; they are also used as SEM imaging signals which are more sensitive to the atomic number. The information conveyed by the backscattered electrons can often be more easily interpreted and it is less dependent on the surface disturbances (e.g., charging).[8,9]

The ratio of number of emitted electrons with kinetic energy $E > 50$ eV to the number of incident electrons is defined as the backscattering coefficient, η, and the ratio for $E < 50$ eV is known as secondary electron yield, δ. The total electron yield is then given as $\sigma = \eta + \delta$.[10] These emission yields are very useful and fundamental for many devices; the application of yields ranges from the plasma thrusters,[11] Hall effect engines, catalysis,[12] surface science, and chemical analysis.[13] During the last few decades a number of experiments have been conducted to investigate the dependence of backscattering coefficient on atomic number of the sample and primary electron energy. It was noted that η increases with atomic number Z for energies greater than 10 keV.[14–16] The general trend of the primary energy dependence of backscattering coefficient was also noted as[17–19] (a) for low Z solids ($Z < 20$), it decreases with increase of primary energy; (b) for high Z elements ($Z > 26$), it increases with primary energy; (c) for intermediate-Z elements, it is almost constant.[20] For many elemental solids and compounds, those historical measurement data were compiled into a database by Joy,[21] and another extended database of backscattering coefficient has been provided very recently.[22] All the reported experimental data were collected in the databases without judging the reliability, and considerable inconsistency found among the different data sources was not looked into. El Gomati *et al.* have considered that at low primary energies η would be surface sensitive to oxidation.[23] While only the surface condition to the secondary electron yield is known to be critical, the surface effect to the measured η values has long been underestimated. And in validation works of Monte Carlo simulation models,[24] the surface effect presented in the experimental data has usually been ignored.

The simulation of electron trajectory using Monte Carlo method is an effective theoretical tool for the study of electron beam-specimen interaction in electron probe related techniques, including surface electron spectroscopy and electron microscopy.[25–27] Not only the energy spectra and yields of emitted electrons can be simulated,[28–30] but also the scanning electron microscopic images of surface morphology of a 3D specimen structure can be modeled[31–36] which allows the wide application of Monte Carlo simulation methods in materials science and semiconductor industry. Backscattering coefficient and secondary yield data are very important for characterizing the electron solid interaction. To test, a Monte Carlo simulation model and code backscattering yields are used commonly. In our previous works, we have pointed out that even though the backscattering coefficient is less affected by the surface condition of the sample as compared to the secondary yield, but the surface contamination presented in many measurements would definitely cause an obvious effect to the measured values for the light and heavy elemental solids and particularly at low primary energies.[37,38] Therefore, those experimental data collected in the Joy's and Akbari's databases without justifying the surface cleanness by using electron spectroscopic signals cannot be used as a reliable data source. Furthermore, machine learning methods derived electron emission yield curve can also be questionable if the source data itself contain non-negligible systematic error.

During the recent years, our knowledge about the electron interaction with solids is becoming more and more rich. Recently, Monte Carlo modeling of electron beam interaction with solids and surfaces has been continuously improved by using up-to-date theories and knowledge of electron scattering within matter; a number of methods based on Monte Carlo models were proposed by different researchers.[28,37,39–47] The most difficult problem in a Monte Carlo modeling was about the description of electron inelastic scattering in a realistic sample; this issue has been partly solved with a formulation of an extended dielectric function[48] in a dielectric approach to electron inelastic scattering. Using experimental data of optical constants, the complex electronic excitation process in any solids can be well treated in a universal and simple way but still with quite accuracy. We have verified that the Monte Carlo simulated backscattering coefficient based on an up-to-date Monte Carlo model is sensitive to the accuracy of optical constants data set adopted,[49] which can be tested by the sum rules. The behavior of surface contamination effect generally presented in experimentally measured data depends on the atomic number of the sample where the contaminants are usually hydrocarbon: several atomic layers' commination will increase η for a light metal Be and for primary energies below 2 keV,[37] and reduce η for a heavy metal W and for primary energies below 100 keV.[38] At very high energies, the surface effect on electron inelastic scattering can be omitted, and the simulation of electron energy spectrum and the spectrum integration (electron emission yield) can agree with experimental data. Therefore, it is natural to consider that one can build a reliable theoretical database of backscattering coefficient values based on an up-to-date Monte Carlo simulation model once the accurate optical constants are available.

A model with higher accuracy has been developed with which the elastic scattering is based on Mott's electron cross section[50] while the dielectric functional formalism is used for the treatment of electron inelastic scattering.[48] The developed classical trajectory Monte Carlo (CTMC) simulation model and the corresponding codes were then successfully used for the calculations in scanning electron microscopy,[31,32,34] Auger electron spectroscopy/microscopy and x-ray photoelectron spectroscopy.[27] In recent years, we have also developed a reverse Monte Carlo analysis method for extraction of the optical constants data from experimentally measured reflection electron energy loss spectroscopy spectra, which was proved to have a very high accuracy via the sum rule tests,[51] to enable highly accurate Monte Carlo simulation of electron beam interaction with a matter. Furthermore, another previous work has clearly indicated the effect of ELFs at the different levels of accuracy on the backscattering coefficient.[49]

The aim of the present work is, hence, to derive the more reliable calculated backscattering coefficient data of the three medium

06 December 2024 01:20:56

© Author(s) 2024

atomic number elements, Cr ($Z = 24$), Co ($Z = 27$), and Pd ($Z = 46$) by using our up-to-date CTMC-SEM Monte Carlo simulation model, where the data accuracy of the backscattering coefficient is associated with the sum rule tests of the ELF used. First, we used different ELF data sets as input to calculate the inelastic cross sections. The ELF data include those taken from the Palik's handbook in which the optical constants data were measured by optical methods[52] and those extracted from experimental reflection electron energy loss spectroscopy (REELS) spectra.[53] The data compiled in the Palik's database were usually measured by different groups under different conditions. The quality of these combined data in a full photon energy range can be evaluated by using sum rule tests. For each element, we will present the backscattering coefficients calculated with different ELFs in the incident energy range of 0.1–100 keV.

A. Monte Carlo model

A Monte Carlo simulation model of electron interaction with solid consists of two types of modeling: elastic and inelastic scattering modeling. Our recent Monte Carlo simulation model covers both elastic and inelastic scatterings. The details of the model are described elsewhere;[37,38] here, we briefly introduce our calculation method.

B. Electron elastic scattering

For elastic scattering calculation, there are two available methods: Mott's cross section and screened Rutherford formula.[28] But, it is known that Mott's relativistic quantum mechanical cross section[50] is very accurate from very high electron energies down to very low energies. So, we have applied Mott's elastic cross sections in our Monte Carlo simulations. The formula for differential elastic cross section is defined as

$$\frac{d\sigma_e}{d\Omega} = |f(\theta)|^2 + |g(\theta)|^2, \tag{1}$$

where σ_e represents total elastic cross section and θ stands for the polar angle of electron scattering into the solid angle of $\Omega - \Omega + d\Omega$. The scattering amplitudes $f(\theta)$ and $g(\theta)$ can be obtained from partial wave expansion method as

$$f(\theta) = \frac{1}{2ik}\sum_{l=0}^{\infty}\left\{(\ell+1)\left(e^{2i\delta_\ell^+} - 1\right) + \ell\left(e^{2i\delta_\ell^-} - 1\right)\right\}P_\ell(\cos\theta), \tag{2}$$

$$g(\theta) = \frac{1}{2ik}\sum_{\ell=1}^{\infty}\left\{-e^{2i\delta_\ell^+} + e^{2i\delta_\ell^-}\right\}P_\ell^1(\cos\theta), \tag{3}$$

where δ_l^+ and δ_l^- represent the spin-up and spin-down phase shifts, respectively, of the ℓth partial wave. $P_\ell(\cos\theta)$ is the Legendre function and $P_\ell^1(\cos\theta)$ is the first order associated Legendre function. Electron exchange potential, electrostatic interaction potential, and correlation-polarization potential are considered in our calculations.[54]

Fermi distribution and Dirac-Fock electron density[55] are used for nuclear and electronic charge-density calculations. We also considered the correlation-polarization potential and the Furness–McCarthy exchange potential[56] which are based on local-density approximation.[57] ELSEPA computer code[54] was used for calculation of Mott's cross section. From the calculated total elastic scattering cross section σ_e, one then obtains the elastic scattering mean free path (EMFP), $\lambda_e = 1/(n_a\sigma_e)$, where $n_a = N_A\rho/A$ represents the atomic number density of the material, N_A is Avogadro's constant, ρ is the density, and A is atomic weight. Figure 1 shows the obtained EMFPs of 192 total cross-sectional data sets. In the low and intermediate energy range, one can see obvious variation among these 192 data sets. These variations should affect the lower energy electron transport and hence the simulated backscattering coefficient results.

C. Electron inelastic scattering

For electron inelastic scattering cross-section calculation, the dielectric functional approach was used. For incident electrons, the differential inverse inelastic mean free path (DIIMFP) is given as[58]

$$\frac{d^2\lambda_{in}^{-1}}{d(\hbar\omega)dq} = \frac{2\gamma^2}{1+\gamma}\frac{1}{\pi a_0 E}\mathrm{Im}\left\{\frac{-1}{\varepsilon(q,\omega)}\right\}\frac{1}{q}, \tag{4}$$

where $\gamma = 1 + E/(m_0c^2)$ is the relativistic correction factor, $2\gamma^2/(1+\gamma)$ is the coefficient which is because of the relativistic effect; a_0 represents the Bohr's radius, and λ_{in} represents the electron IMFP. $\varepsilon(q,\omega)$ is the complex dielectric function of medium, $\hbar\omega$ is the energy loss, and $\hbar q$ is momentum transfer for the electronic excitation. $\mathrm{Im}\{-1/\varepsilon(q,\omega)\}$ is the ELF which characterizes inelastic scattering. Penn proposed an algorithm for determining momentum transfer dependent ELF, where he expanded optical ELF $\mathrm{Im}\{-1/\varepsilon(\omega)\}$, at $q = 0$ to finite q according to the Lindhard ELF. By using Lindhard dielectric function, $\varepsilon_L(q,\omega;\omega_p)$, the expanded ELF is given as

$$\mathrm{Im}\left\{\frac{-1}{\varepsilon(q,\omega)}\right\} = \int_0^\infty g(\omega_p)\mathrm{Im}\left\{\frac{-1}{\varepsilon_L(q,\omega;\omega_p)}\right\}d\omega_p, \tag{5}$$

where $g(\omega)$ is termed as the expansion coefficient, and it is associated to the optical ELF by

$$g(\omega) = \frac{2}{\pi\omega}\mathrm{Im}\left\{\frac{-1}{\varepsilon(0,\omega)}\right\}. \tag{6}$$

Two well-known sum rules, the oscillator strength sum rule (f-sum rule) and the perfect screening sum rule,[59] were used to check the reliability of the optical ELF data. The f-sum rule is calculated as

$$Z_{eff} = \frac{2}{\pi\Omega_P^2}\int_0^{\omega_{\max}}\omega\mathrm{Im}\left\{\frac{-1}{\varepsilon(\omega)}\right\}d\omega, \tag{7}$$

where $\hbar\Omega_P = \sqrt{4\pi n_a e^2/m}$. At the limit of $\omega_{\max} \to \infty$, the f-sum rule results of Z_{eff} should be equal to the total number of electrons per atom or per molecule. The Kramers–Kronig relation[60] is used

06 December 2024 01:20:56

© Author(s) 2024

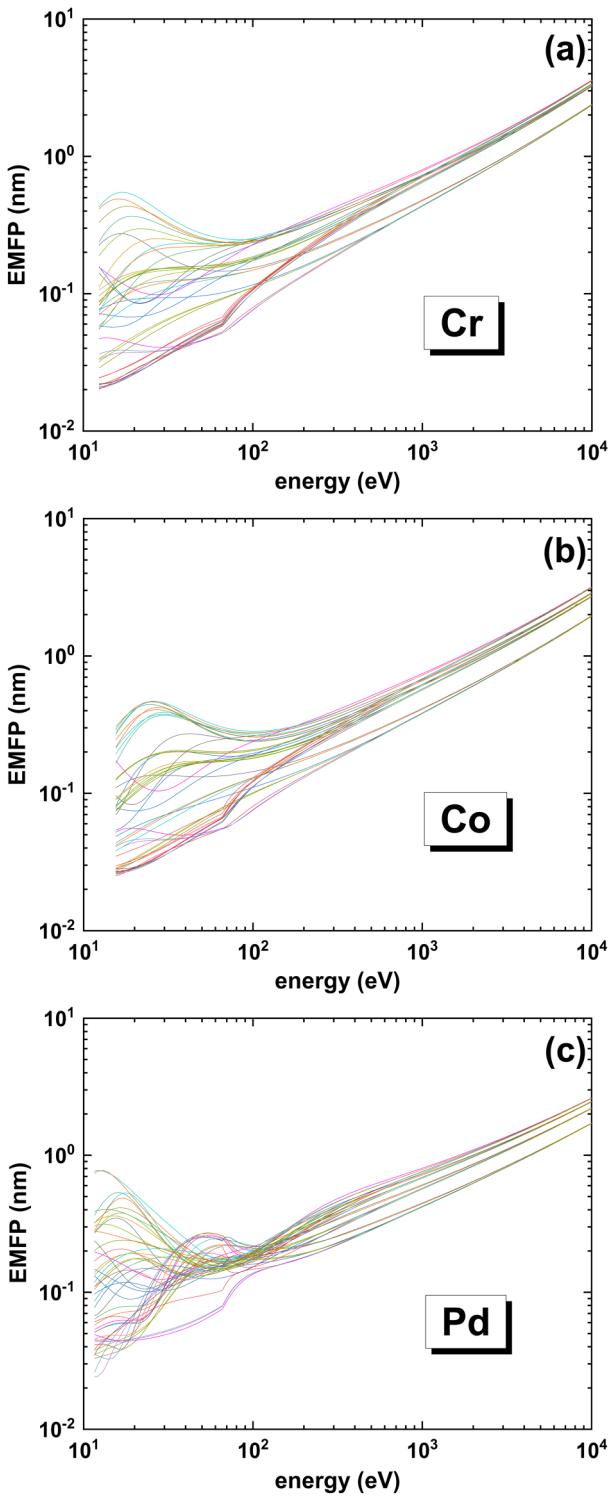

FIG. 1. Calculated electron EMFPs as functions of electron kinetic energy by using 192 scattering potential models for (a) Cr, (b) Co, and (c) Pd.

to calculate perfect screening sum rule as

$$P_{\text{eff}} = \frac{2}{\pi}\int_0^{\omega_{\max}} \frac{1}{\omega}\,\text{Im}\left\{\frac{-1}{\varepsilon(\omega)}\right\}d\omega + \text{Re}\left\{\frac{1}{\varepsilon(0)}\right\}, \tag{8}$$

where $\text{Re}\{1/\varepsilon(0)\} = 0$ for conductors. The *ps*-sum rule result of P_{eff} is unity when the limit of $\omega_{\max} \to \infty$. The perfect screening sum rule is dominated by the low energy loss region of the ELFs data due to the ω^{-1}-factor in the integrand. On the other hand, because of the ω-factor, the *f*-sum rule is dominated by the high energy loss regions. Therefore, these sum rules can be used to verify the accuracy of ELF in the whole energy loss range.

D. Monte Carlo simulation

Electron penetration within a material suffers elastic and inelastic collision. There will be only change in the direction of motion of an electron when it has elastic collision, while during inelastic collision, an electron will not only change the direction of movement but will lose some energy as well. In our simulation, Mott's cross section describes the elastic collision, while inelastic collision is described by the dielectric functional approach. Differential cross sections will be used to calculate the scattering angle and energy loss during a collision. The kinetic energy after an inelastic collision will be reduced by $\hbar\omega$. If the energy loss $\hbar\omega$ is smaller than the binding energy of the outermost inner-shell, $\hbar\omega < E_B$ (where E_B refers to the binding energy of the lowest identifiable inner-shell ionization edge in the plot of optical ELF), then a secondary electron is supposed to be excited from the Fermi sea by the transfer of an energy equals to $\hbar\omega$ from the primary electron to a valence electron where the excitation probability will be proportional to a combined density of states of free electrons. If $\hbar\omega > E_B$, a secondary electron having kinetic energy $\hbar\omega - E_B$ is excited from the inner-shell.[30] The relaxation of the ionized atom may cause: the emission of an Auger electron or the emission of a photon. However, the influence of Auger electrons to the backscattering coefficient is insignificant due to the lower probability of the inner-shell ionization.

After experiencing number of elastic and inelastic scattering collisions within the sample under study, some of the electrons will reach to the surface. These electrons have a certain probability to escape from the surface of the sample, i.e., the transmission function *T*. In our work, we used the quantum mechanical transmission function given as[28]

$$T(E,\beta) = \begin{cases} \dfrac{4\sqrt{1 - U_0/E\cos^2\beta}}{\left[1 + \sqrt{1 - U_0/E\cos^2\beta}\right]^2}, & \text{if } E\cos^2\beta > U_0, \\ 0, & \text{otherwise.} \end{cases} \tag{9}$$

In the above formula, β represents the angle between the direction of electron and the surface normal and U_0 is termed as the surface barrier which is equal to the sum of Fermi energy and work function. The work function values used for three metals, Cr, Co, and Pd are respectively 4.6, 5.0, and 5.4 eV. On the basis of the kinetic energy, an escaped electron can be divided into a true secondary electron (less than 50 eV) or a backscattered electron

06 December 2024 01:20:56

© Author(s) 2024

TABLE I. The optical ELF data used for Cr.

Element	ELF name	Photon energy range and the corresponding data set			
Cr	Tanuma	0.04–29.5 eV (Tanuma *et al.*[70])	30–35 eV interpolation	36 eV–30 keV (Henke *et al.*[67])	30 keV–10 MeV
	Palik	0.04–9999 eV (Palik[66])		10 keV–30 keV (Henke *et al.*[67])	EPDL97
	Yang	0.1–200 eV (Yang *et al.*[69])	201–203 eV interpolation	204 eV–30 keV (Henke *et al.*[67])	(Cullen *et al.*[68])

(greater than 50 eV). The electrons having energy higher than 50 eV are thus counted for the calculation of the backscattering coefficient.

E. Energy loss function data

The ELF illustrates valence and inner-shell electrons excitation in a solid, which is liable for the process of electron energy loss with the energy transfer $\hbar\omega$ and momentum transfer $\hbar q$. It is the most important quantity for the present Monte Carlo simulation, and the accuracy of this quantity will play the most vital role for the reliability of simulated data. Due to the complexity of electronic excitation in a realistic material, it is very hard to obtain the accurate ELF from a first-principles theoretical calculation at present. The experimentally measured data in the optical limit of $q \rightarrow 0$ have been mostly used in the Monte Carlo simulations[28,40,61,62] as well as in the calculations of electron IMFP and stopping power.[63–65]

In Palik's database of optical constants,[66] there are usually several data sets for one element; these data sets are either in the separated ranges of photon energy $\hbar\omega$ (or electron energy loss) or in somewhat overlapped ranges. Then, we have combined them together with high energy $\hbar\omega$ data[67,68] to form a unique optical ELF data set, named as "ELF-Palik." Other combined ELFs are similarly named as "ELF-Yang,"[69] "ELF-Tanuma,"[70] and "ELF-Werner."[53] All the sources of these data sets are listed in Tables I–III for Cr, Co, and Pd, respectively, and the corresponding ELF plots are shown in Fig. 2. The linear interpolation was made for ELFs through refractive index n and extinction coefficient k when data are missing within a large gap. The "ELF-Tanuma" is in fact used in their calculation of IMFP,[70] while the source of data has not been explicitly mentioned. The ELFs in the intermediate energy loss region for "ELF-Yang" and "ELF-Werner" are derived from their analysis of REELS spectra. Although Tanuma *et al.* have depicted that their ELF data are same as that of "ELF-Palik," but it can be seen that in the range of 30–60 eV for Cr and 40–70 eV for Pd, their data are somehow different from the original data in the Palik's database, perhaps due to the interpolation procedure used. In case of Co, Tanuma *et al.* have depicted that data they used are same as that of "ELF-Werner," but they actually differ in the range of 70–100 eV.

Figure 3 shows the sum rule integration results of Eqs. (7) and (8) as functions of the integration upper limit, $\hbar\omega_{max}$, for the ELFs of these three elements. For very large $\hbar\omega_{max}$, the integration value converges to the sum rule results. Corresponding *f*-sum and the *ps*-sum rule values are shown in Table IV. Note that for different ELF data sets, the sum rule values are quite different. In the case of Cr, the relative errors of both *f*- and the *ps*-sum rules are quite small for "ELF-Yang;" while for "ELF-Palik" and "ELF-Tanuma," one of the errors of the *f*- and the *ps*-sum rules is smaller and the other one is greater. For Co, "ELF-Yang" would be the best because both sum rules are almost perfect, and "ELF-Werner" and "ELF-Tanuma" are also good while "ELF-Palik" is seen unacceptable, indicating that the inelastic scattering probability would be underestimated with "ELF-Palik." For Pd, "ELF-Yang" is also better even though the *f*-sum error is a little larger but the *ps*-sum is quite small; "ELF-Werner" is reasonably good. "ELF-Tanuma" and "ELF-Palik" have nearly perfect *f*-sum but quite worse *ps*-sum, indicating the overestimation at low energy losses. Because the *ps*-sum rule error is dominated by the accuracy of the lower energy part of ELF and the *f*-sum rule error is dominated by the higher energy part, then different energy loss regions being high or low are emphasized in different sum rules. Nevertheless, this is anyhow a simple overall estimation; the accuracy of an ELF in a certain short energy loss range cannot be known definitely according to the sum rules. It is also necessary to mention that an ELF having a gross error of *ps*-sum, like the cases of "ELF-Palik" for the three metals and "ELF-Tanuma" for Pd, will lead to inaccurate IMFP values in the energy region from the low energy up to very high energies due to the integration over the whole allowed energy loss range. But, the larger error of *f*-sum and smaller error of *ps*-sum only affect the accuracy of IMFP values at high energies. Therefore, in a comparison of two ELF data sets that one having a smaller *f*-sum rule error and greater *ps*-sum rule error and another one having a greater *f*-sum rule error and smaller *ps*-sum rule error, like the case of "ELF-Werner" and "ELF-Yang" for Pd, the later one would be better.

06 December 2024 01:20:56

TABLE II. The optical ELF data used for Co.

Element	ELF name	Photon energy range and the corresponding data set			
Co	Werner	0.5–70.5 eV (Werner *et al.*[53])	71–80 eV interpolation	80 eV–30 keV (Henke *et al.*[67])	30 keV–10 MeV
	Tanuma	0.5–70.5 eV (Tanuma *et al.*[70])		72 eV–30 keV (Henke *et al.*[67])	EPDL97
	Palik	0.07–2000eV (Palik[66])		2000 eV–30 keV (Henke *et al.*[67])	(Cullen *et al.*[68])
	Yang	0.1–200 eV (Yang *et al.*[69])	201–203 eV interpolation	204 eV–30 keV (Henke *et al.*[67])	

© Author(s) 2024

TABLE III. The optical ELF data used for Pd.

Element	ELF name	Photon energy range and the corresponding data set			
Pd	Werner	0.5–70.5 eV (Werner *et al.*[53])	71–80 eV interpolation	80 eV–30 keV (Henke *et al.*[67])	30 keV–10 MeV
	Tanuma	0.1–17.26 eV (Tanuma *et al.*[70])	18–120 eV interpolation	122 eV–30 keV (Henke *et al.*[67])	EPDL97
	Palik	0.01–525.4 eV (Palik[66])		526 eV–30 keV (Henke *et al.*[67])	(Cullen *et al.*[68])
	Yang	0.1–200 eV (Yang *et al.*[69])	201–203 eV interpolation	204 eV–30 keV (Henke *et al.*[67])	

II. RESULTS AND DISCUSSIONS

The electron IMFP, $\lambda_{in}(E)$, is defined as the average distance coved by an electron between two successive inelastic collisions; it is reciprocal to the inelastic scattering cross section and is calculated by the double integration of DIIMFP in Eq. (4), where $E - E_F$ is the upper limit of integration over the energy loss $\hbar\omega$. E represents the kinetic energy of the electron measured from the bottom of valence band and E_F represents the Fermi energy. Greater IMFP means that the electron can travel a longer distance before it loses an energy, implying elastic scattering is more important. So, the probability of electron to be backscattered will be higher. Backscattering coefficient, $\eta(E_p)$, dependence on primary energy E_p can then be explained from the IMFP behavior on kinetic energy E later.

Figure 4 shows the calculated $\lambda_{in}(E)$ curves for the three elements with the different optical ELF data sets. In Fig. 4(a) for Cr, it can be seen that the two IMFP curves, "IMFP-Tanuma" and "IMFP-Palik," have no intersection and the "IMFP-Palik" curve is always lower than the "IMFP-Tanuma" curve from the low energy region to the high energy region. While the "IMFP-Yang" and "IMFP-Tanuma" curves intersect at about 200 eV above which the "IMFP-Tanuma" is always greater than the "IMFP-Yang." The behavior of the difference between IMFPs with three optical ELFs is consistent with the sum rule results of the ELFs shown in Table IV. Because the *ps*-sum rules for "ELF-Palik" and "ELF-Tanuma" are overestimated while the *f*-sum rules of them are underestimated, the resultant "IMFP-Palik" and "IMFP-Tanuma" are then both underestimated in the low energy region and overestimated in the high energy region. Comparatively, the "IMFP-Yang" should be quite reasonable in the low energy region because of the excellent *ps*-sum rule result of ∼0.3% and be only slightly overestimated in the high energy region considering the error of *f*-sum rule of ∼2.3%.

In the case of Co, the "IMFP-Tanuma" and "IMFP-Werner" curves in Fig. 4(b) are nearly overlapped because their ELF data sets almost agree. The "IMFP-Palik" curve is higher than other three curves above 30 eV as the "ELF-Palik" has quite low intensity [Fig. 2(b)] and the sum rule values are underestimated. Because almost perfect sum rules of "ELF-Yang," the corresponding "IMFP-Yang" should be the ideal one; however, it is not very different from "IMFP-Tanuma" and "IMFP-Werner" because the sum rules of "ELF-Tanuma" and "ELF-Werner" are also good.

For Pd in Fig. 4(c), such an analysis becomes a little bit complex because of the sum rule errors for different ELFs. Comparatively, the accuracy of "IMFP-Yang" for Pd is similar as that for Cr and would be still satisfactory in the low energy region because of the excellent *ps*-sum rule result with an error of ∼0.3% and be only slightly underestimated in the high energy region considering the error of *f*-sum rule of ∼2.8% for "ELF-Yang." Though the *f*-sum rules for "ELF-Tanuma" and "ELF-Palik" are excellent but their *ps*-sum rules are quite bad, with an error of ∼13%, resulting the much underestimation of "IMFP-Tanuma" and "IMFP-Palik;" due to the integration over the whole energy loss range, this underestimation has presented its effect not only in the low energy region but also in the high energy region. As mentioned previously, "ELF-Yang" is more preferential than "ELF-Werner" for the smaller *ps*-sum rule error. The "IMFP-Yang" curve intersects with the "IMFP-Werner" curve at about 40 eV above which the "IMFP-Werner" curve is lower. Therefore, the overestimation of "ELF-Werner" is likely to happen for $\hbar\omega > 40$ eV. This relates to the simulated electron backscattering coefficient behavior shown later.

The Monte Carlo simulations for the energy spectra of backscattered electrons for primary electrons normally incident on the ideal smooth and clean surfaces of Cr, Co, and Pd have been performed at first. The calculated range of primary electron energy E_p is from 0.1 to 100 keV. Figure 5 demonstrates the simulated backscattering $N(E)$ spectra. In each simulation, totally 1×10^7 primary electron trajectories were traced.

The backscattering coefficient value, $\eta(E_p)$, is then obtained by integrating $N(E)$-spectrum over the kinetic energy E of emitted electrons for each primary electron energy E_p. Therefore, the backscattering coefficient at each E_p is actually contributed by electrons having varied energies with their corresponding IMFPs, $\lambda_{in}(E)$, shown in Fig. 4. At a low primary energy, only the lower energy electrons can play a role, and, the low loss in ELF dominates IMFP and *ps*-sum rule is more effective. At a high primary energy, not only the low energy electrons but also the high energy electrons contribute to backscattering coefficient, and, therefore, both the *f*-sum rule and *ps*-sum rule become effective. Figure 6 shows the simulated backscattering coefficients by using different ELF data sets for the three elemental solids. The comparison with the experimental data is also made.

For Cr, the calculated backscattering coefficient curves in Fig. 6(a) with the three different ELFs show the similar trend of variation with E_p; however, their values are somewhat different. The variation of η value relates to sum rules via IMFP. Clearly, a larger IMFP would result in a greater η value because of less frequent electron inelastic scattering during electron transport. As the *ps*-sum rule for "ELF-Yang" is excellent and *f*-sum rule is also very good, the backscattering coefficient calculation should be very reasonable and the best among the three calculated data. Indeed, Fig. 6(a) shows that "η-Yang" approaches the experimental data of

06 December 2024 01:20:56

© Author(s) 2024

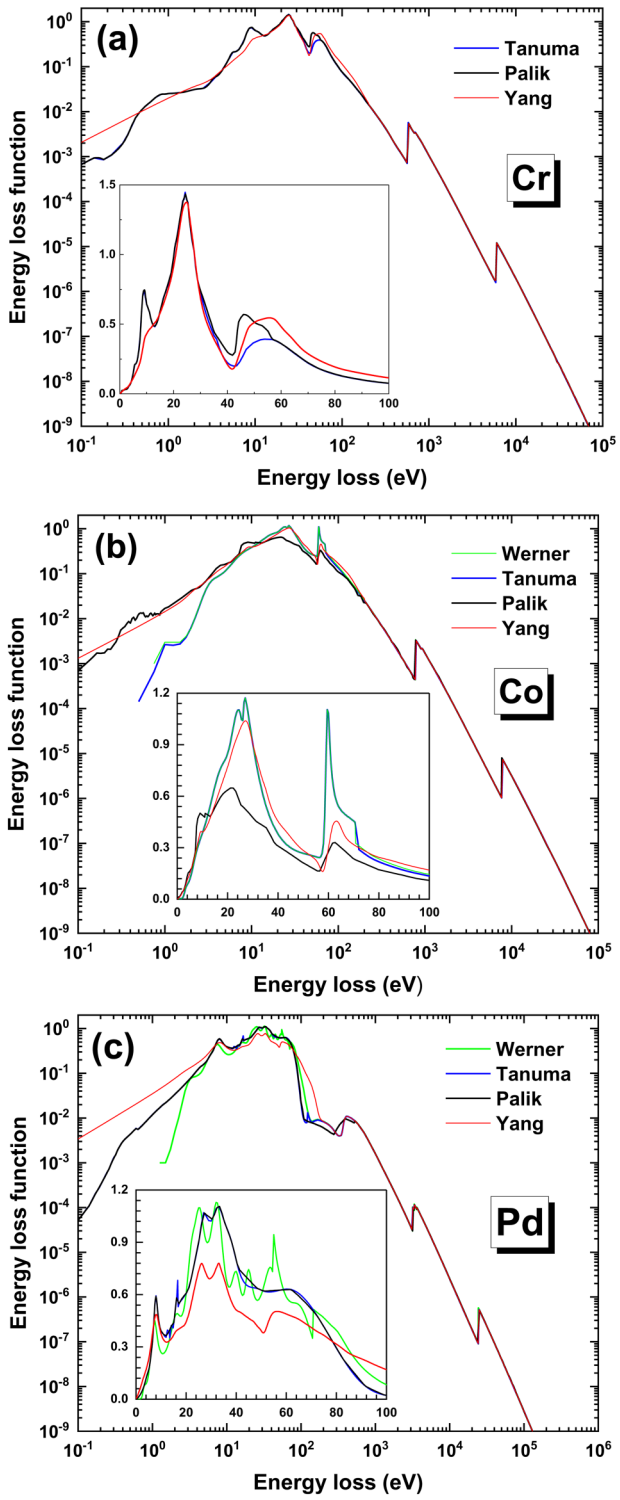

FIG. 2. The optical ELFs of (a) chromium, (b) cobalt, and (c) palladium, where the data sources are described in Tables I–III, respectively.

Heinrich[71] and Bishop[72] at very high primary energies above 10 keV. For "ELF-Palik," the overestimated *ps*-sum rule and underestimated *f*-sum rule indicate that the "IMFP-Palik" is underestimated at low energies and overestimated at high energies and so forth "η-Palik" at corresponding primary energies. For "ELF-Tanuma," the ploarities of sum rule errors are quite similar to those of "ELF-Palik" except the magnitudes are different. The larger error of *f*-sum rule results in the more overestimated "η-Tanuma" at high primary energies.

For Co in Fig. 6(b), the two curves, "η-Tanuma" and "η-Werner," are very close because the sum rule errors for "ELF-Tanuma" and "ELF-Werner" are small and close. While the *ps*-sum rule error for "ELF-Yang" is even smaller and nearly perfect, then the calculated "η-Yang" should be the most accurate particularly at low energies. Indeed, all the three data, "η-Yang," "η-Tanuma," and "η-Werner" agree at high primary energies and agree with experimental data of Heinrich[71] above 20 keV. It is easy to see that the "η-Palik" curve is too much overestimated in comparison with experiments because both the sum rules for "ELF-Paillk" are underestimated and, hence, the ELF intensity in the whole energy loss range is much weakened and so forth the inelastic scattering probability. From the above results, we can say that the sum rule analysis is very useful for verifying the data quality of a Monte Carlo simulation while using the optical ELF for modeling the inelastic scattering of electrons.

For Pd in Fig. 6(c), the four ELF data sets have resulted the similar values of the calculated backscattering coefficients at high primary energies above 10 keV, which close to the experimental data of Heinrich[71] above 20 keV; this is clear because their *f*-sum rules are all good. But, only the "ELF-Yang" has nearly perfect *ps*-sum rule while the "ELF-Werner" has error ~5.5% and "ELF-Tanuma" and "ELF-Palik" have even larger error ~13.0%. Therefore, at low primary energies, only the "η-Yang" is considered to be accurate and "η-Werner," "η-Tanuma," and "η-Palik" should all be underestimated below 10 keV. But, this consideration raises a question in comparison with experimental data of Heinrich[71] at 10 keV: it seems that the lower η-value is likely to be more reasonable. For answering this question, we need to consider two possible uncertainties in making such a comparison. The first one is the theoretical uncertainty coming from the choice of Mott's electron elastic scattering cross section. In a previous calculation of secondary electron yield and backscattering coefficient for Si, it has been shown that the effect of the scattering potential model on secondary electron yield can be very large, but it is small on backscattering coefficient.[76] As it has been illustrated in Fig. 1 that the calculated the differences among EMFPs for 192 scattering potential models are small; therefore, it can be expected that this theoretical uncertainty on backscattering coefficient could be also small. We have then also performed additional calculations by using 192 different elastic cross-section models with the ELSEPA code. Figure 7 shows these 192 $\eta(E_p)$-curves for each element. Indeed, the obtained results do not show large difference above several keV. However, the variance becomes larger by decreasing primary energy down to below 1 keV.

On the other hand, the second uncertainty comes from the possible systematic uncertainty involved in experimental measurements. The previous studies[37,38] have suggested that the carbon

06 December 2024 01:20:56

© Author(s) 2024

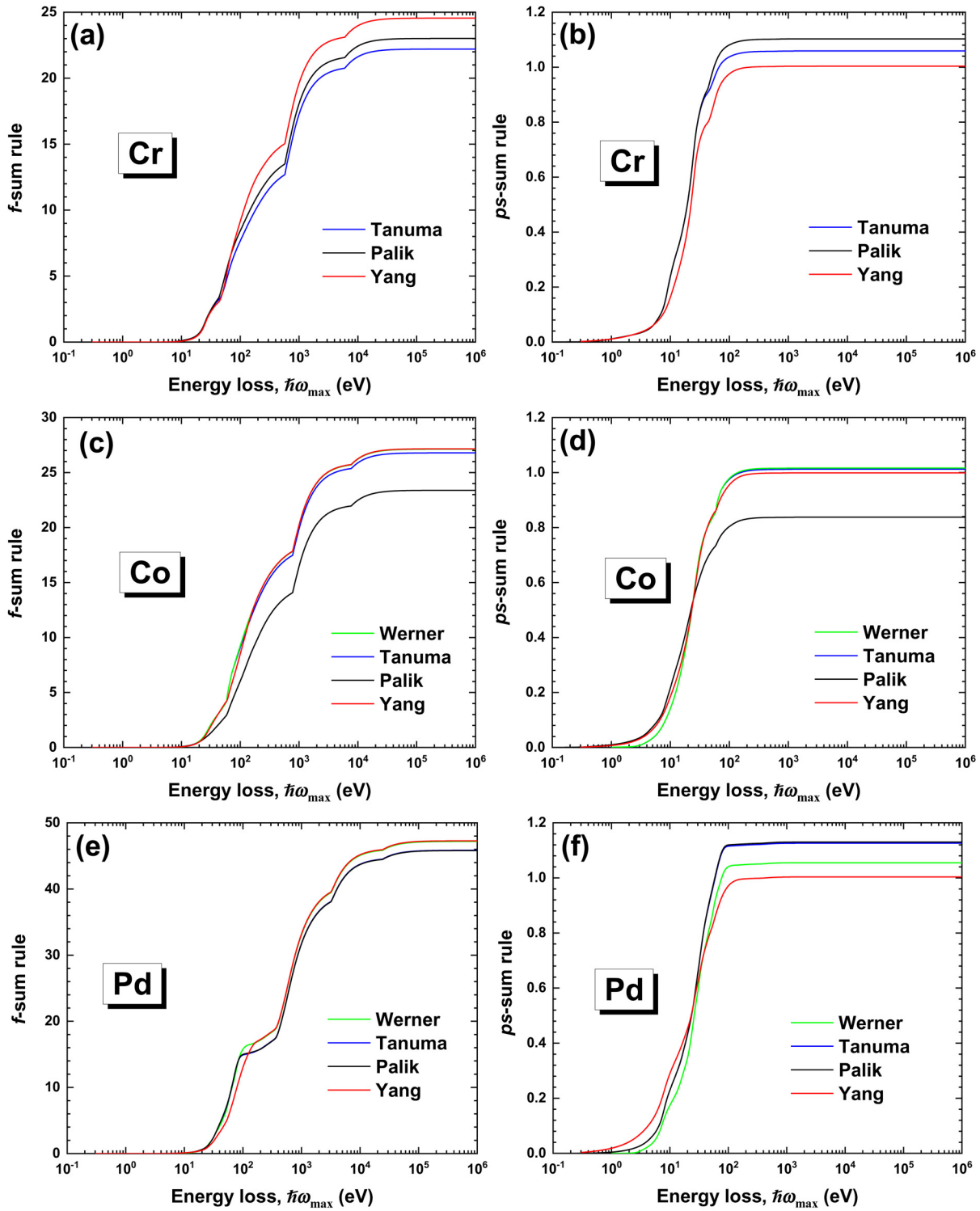

FIG. 3. The *f*- and *ps*-sum integrations as functions of the integration upper limit, $\hbar\omega_{max}$, in Eqs. (7) and (8) for (a) and (b) chromium, (c) and (d) cobalt, and (e) and (f) palladium, respectively.

06 December 2024 01:20:56

© Author(s) 2024

TABLE IV. The f- and ps-sum rules and their relative errors for Cr, Co, and Pd.

		f-sum rule		*ps*-sum rule	
Elements	ELF	Value	Relative error (%)	Value	Relative error (%)
Cr	Tanuma	22.20	−7.5	1.05	5.9
	Palik	23.01	−4.1	1.10	10.3
	Yang	24.55	2.3	1.003	0.3
Co	Tanuma	26.79	−0.8	1.01	1.2
	Werner	27.13	0.5	1.01	1.7
	Palik	23.39	−13.3	0.83	−16.2
	Yang	27.16	0.6	0.9991	−0.1
Pd	Werner	47.20	2.6	1.05	5.5
	Tanuma	45.85	−0.3	1.12	13.0
	Palik	45.81	−0.4	1.13	13.0
	Yang	47.29	2.8	1.003	0.3

contamination of surface can present an obvious effect on the measured η-values for the light and heavy elemental solids and particularly at low primary energies. It is then very likely to have also an effect for the intermediate-Z elements. In addition to carbon contamination, the effect of water vapor molecules in the chamber of an environmental scanning electron microscope on backscattering coefficient has also been studied.[77] In comparison with the early experimental measurements, the systematic error due to the surface contamination should be considered because the measurements were either performed in condition without ultrahigh vacuum environment and/or absent or insufficient *in situ* surface cleaning. Therefore, the effect of contamination should be studied while performing the simulations. For example, Hunger's experiments were carried out at pressure of 4×10^{-3} Pa in an electron probe microanalyser,[18] and some other measurements[71–73] were performed in 1960s when the ultrahigh vacuum condition was not available. To compare with those experimental data, we have performed the calculations for the Cr, Co, and Pd solids whose surfaces are covered by several amorphous carbon layers. In this work, we considered only amorphous carbon contamination, as the physical properties such as optical constants for other complex adsorbates are mostly unknown. We considered that the effect of the carbon layer can be much higher as compared to the oxidation layer, as it has lower atomic number and also due to the nature of chemical composition of the contamination layer in practice. Amorphous carbon is well known to dominate the contamination ingredient and particularly under electron beam bombardment condition. Its electrical properties have been measured by x-ray photoelectron spectroscopy[78] and its optical data are available.[79] In theoretical point of view, the present simulation is the combination of the best available Monte Carlo technique and the best available ELFs, the simulation results are expected to predicate much more realistic backscattering coefficient data in such an experimental condition. Here, it is worth to mention that experimentally the surface morphology may likely to be changed during the surface cleaning processes via annealing, ion sputtering, or plasma exposure, which in turn also influence the electron emission yield.[80] In this work, we

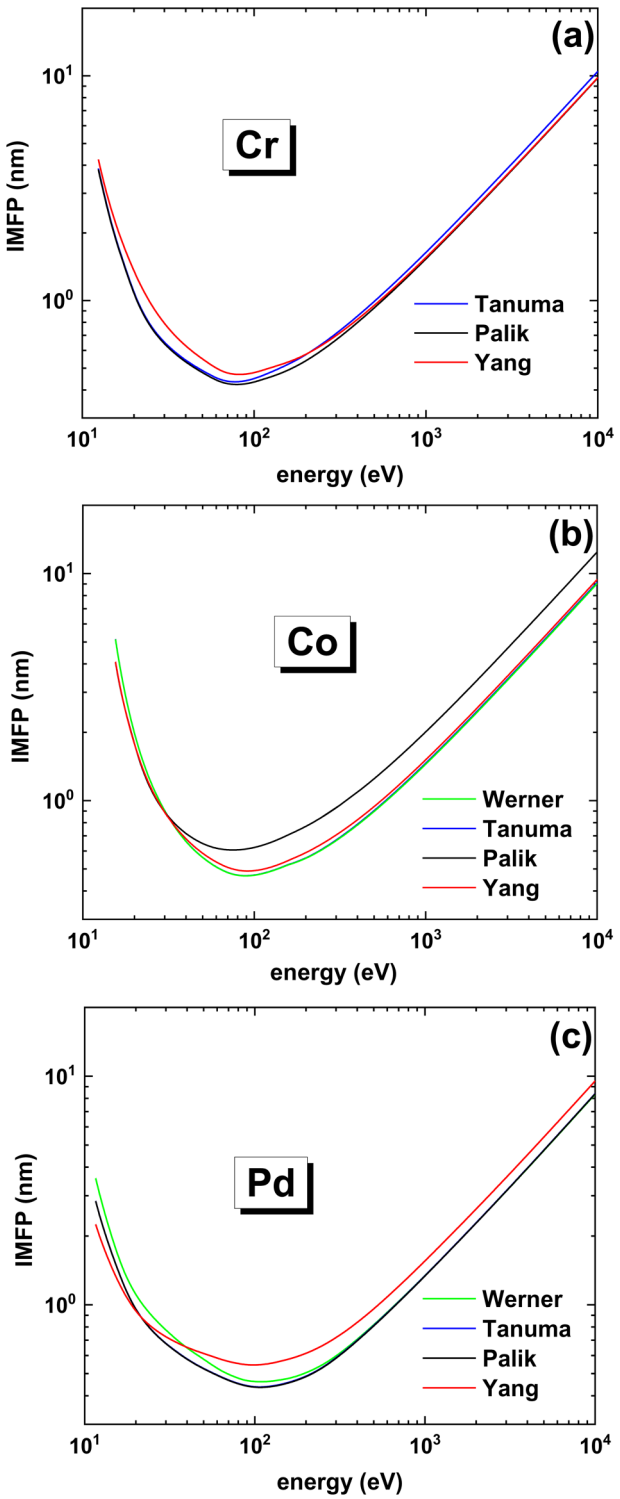

FIG. 4. Calculated electron IMFPs as functions of electron kinetic energy for (a) Cr, (b) Co, and (c) Pd.

06 December 2024 01:20:56

© Author(s) 2024

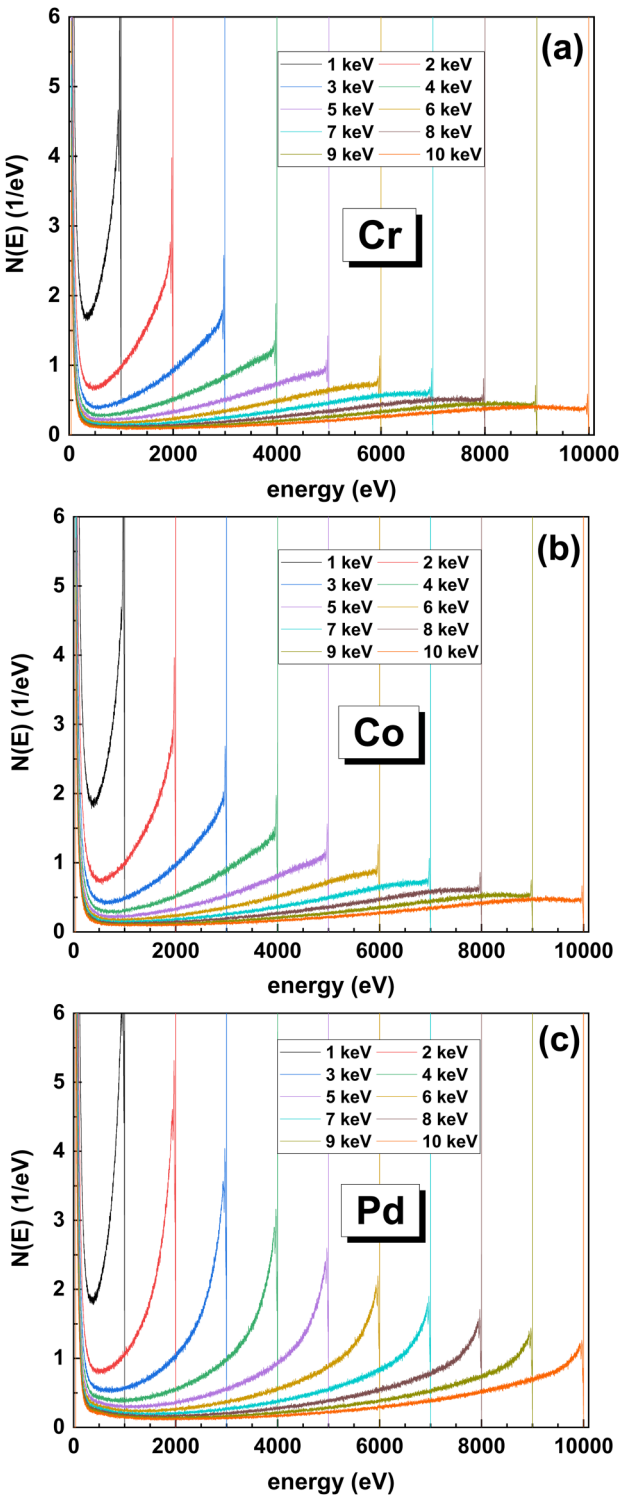

FIG. 5. Monte Carlo simulated electron backscattering energy spectra for (a) Cr, (b) Co, and (c) Pd.

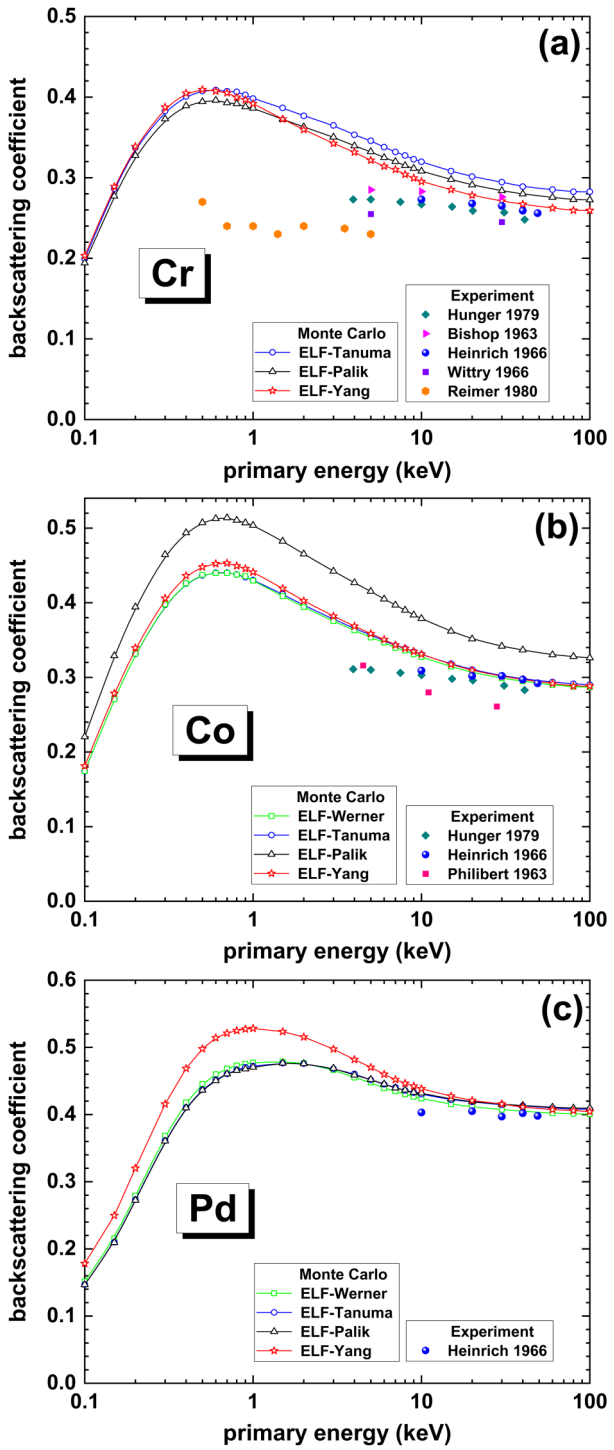

FIG. 6. Comparison between the present Monte Carlo simulated electron backscattering coefficients (solid lines with empty symbols) by using different optical ELF data sets and the experimental data (solid symbols)[18,71–75] for (a) Cr, (b) Co, and (c) Pd.

06 December 2024 01:20:56

© Author(s) 2024

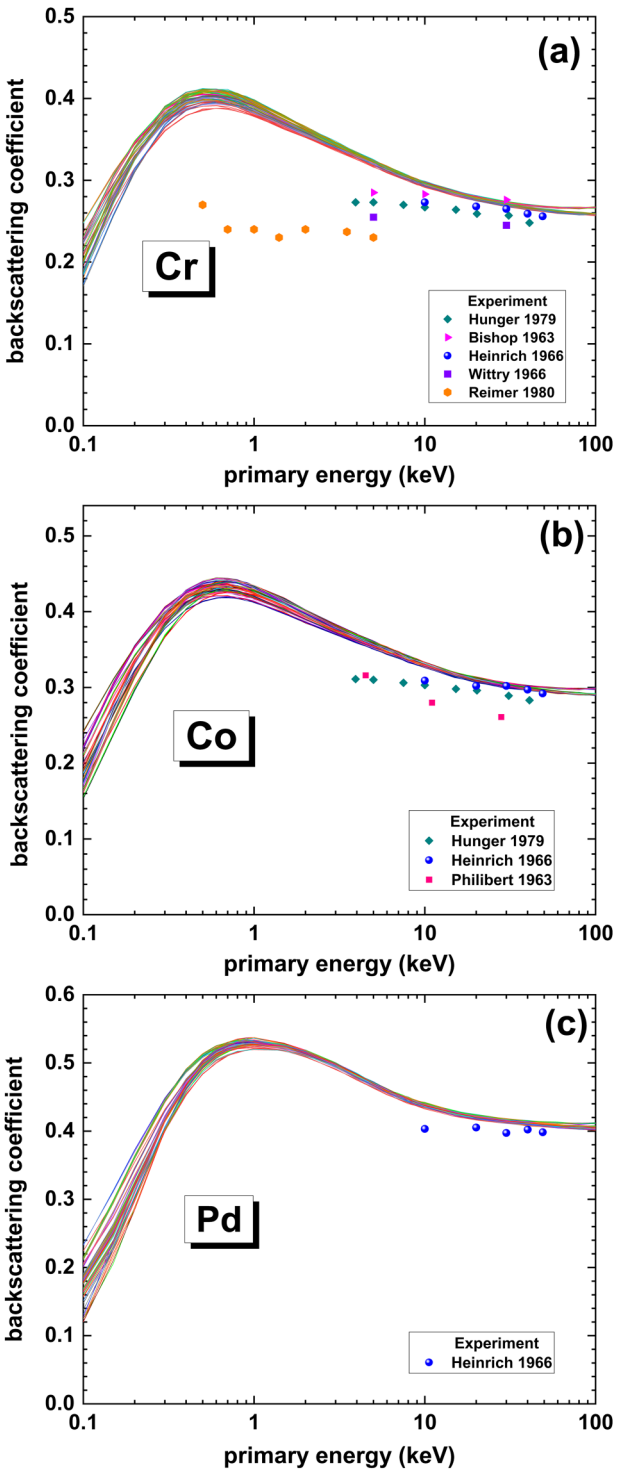

FIG. 7. Monte Carlo simulated backscattering coefficients (solid lines) calculated with "ELF-Yang" and 192 different elastic scattering cross section models for (a) Cr, (b) Co, and (c) Pd.

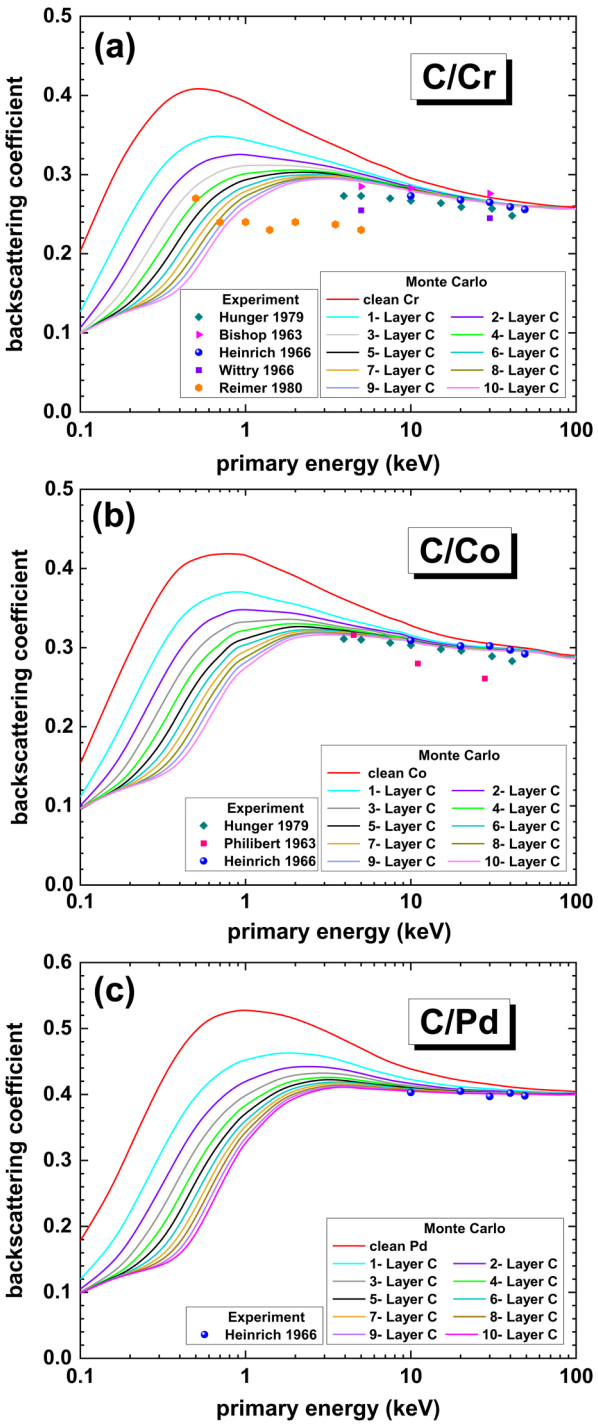

FIG. 8. Comparison on the electron backscattering coefficients between the experimental data (solid symbols)[18,71–75] and the present Monte Carlo simulations calculated with "ELF-Yang" for clean and contaminated (a) Cr, (b) Co, and (c) Pd surfaces, where in the simulation, the contaminated surfaces are covered by different atomic layers (1–10) of amorphous carbon.

06 December 2024 01:20:56

© Author(s) 2024

will ignore the surface morphology and only consider the planar surface.

We also considered amorphous carbon contamination in our work; the mass density of amorphous carbon is 1.900 g/cm^3 and work function value is 5.0 eV. The effect of number of layers of carbon contamination was studied. For this calculation, the ELF used is taken from three different references, ELF from 0 to 200 eV is extracted from a REELS spectrum.[79] In the range of 200 eV–30 keV, ELF was calculated from atomic scattering factor taken from Henke's database.[67] While for the range of 30 keV–10 MeV, we used the atomic scattering factor from EPDL97 database.[68] Here, we used CTMC-ATOMIC[37] simulation code with only bulk excitation model for the calculation of the contaminated surface. The *f*-sum and the *ps*-sum rule values for amorphous carbon are 5.05 and 0.946, respectively. The physical properties of the contamination film, like ELF, work function, bandgap, and density used in this simulation, are similar with those of the solid state of the adsorbates.

Figure 8 shows the comparison of the simulated results for contaminated surfaces with the available experimental data (the actual density value of contamination in a specific experiment is unknown). The "3412"-scattering potential model is used. It can be seen that by covering some carbon atomic layers (where the thickness of one atomic layer of carbon contamination is ∼3.35 Å), the backscattering coefficient is intensively reduced at low primary energies below several keV and tends to approach the experimental data at high primary energies. Above 4 keV, the experimental data measured by different groups are quite consistent with our calculations. The situation is pretty much similar as observed in the case of Mo and W.[38] Unfortunately, there is no experimental data available at lower primary energies for a direct comparison; however, other experimental data for the nearby atomic number elements can be employed to explore the trend. Reimer and Tollkamp have presented a plot for the general trend of backscattering coefficients on primary energy and atomic number.[74] For Cu, their closest solid measured in atomic number to Co, the plot the constant value ∼0.31 down to below 3 keV; and for Ag, the nearby solid in atomic number to Pd, the measured value decreases from ∼0.41 with decreasing primary energy from 10 keV. In addition, it can be seen from the plot in Ref. 38 for Mo, which is also the nearby solid in atomic number to Pd, that several other experiments demonstrate a similar decreasing behavior with decreasing primary energy from 10 keV. The general trend agrees with the present calculation of contamination effect.

The above calculation shows that certainly the contamination effect is as large as expected because of the obvious difference in atomic numbers between the carbon adsorbate and metal substrate; for the intermediate-*Z* elements, the contamination would tend to reduce the backscattering coefficient mainly in the primary energy region of 10^{-1}–10^{0} keV.

III. CONCLUSION

In this work, we have employed an up-to-date Monte Carlo simulation model and investigated the effects of ELF data accuracy and surface contamination on the Monte Carlo simulated electron backscattering coefficients for Cr, Co, and Pd metals in primary energy range of 0.1–100 keV. The comprehensive analysis of *f*- and *ps*-sum rule results illustrates that the *f*-sum rule for ELF emphasizes the accuracy of calculation at high primary energy while *ps*-sum rule conveys the accuracy of calculation in the whole range of primary energy and particularly at low primary energy. The large positive/negative errors of these sum rules can lead to underestimation/overestimation of backscattering coefficient. The present simulation data for pure metals are found to be higher than the available experimental data for these metals except at very high energies above 20 keV. While the calculation results for the carbon contaminated Co and Pd surfaces have shown excellent agreement with the experimental data, indicating that very likely all the available historical experimental data of backscattering coefficient suffer the contamination effect. Therefore, the Monte Carlo simulation technique can be used to establish a reliable theoretical database of electron backscattering coefficients for ideal elemental solid surfaces, which are free of the harmful factors, before further comprehensive experimental data measured for clean surfaces are available.

ACKNOWLEDGMENTS

S. F. Mao acknowledges the National MCF Energy R&D Program of China (Grant No. 2019YFE03080500) and the Collaborative Innovation Program of Hefei Science Centre, CAS (Grant No. 2022HSC-CIP010). Y. B. Zou acknowledges the Natural Science Foundation of Xinjinag Uygur Autonomous Region (Grant No. 2022D01A223). Z. J. Ding acknowledges the Chinese Education Ministry through "111 Project 2.0" (No. BP0719016). We thank Professor H. M. Li and the supercomputing center of USTC for the support of parallel computing.

AUTHOR DECLARATIONS

Conflict of Interest

The authors have no conflicts to disclose.

Author Contributions

H. I. Imtiaz: Formal analysis (equal); Investigation (equal); Visualization (equal); Writing – original draft (equal). **M. S. S. Khan:** Investigation (supporting). **A. Hussain:** Investigation (supporting). **S. F. Mao:** Funding acquisition (equal); Methodology (supporting); Software (supporting). **Y. B. Zou:** Funding acquisition (equal); Investigation (supporting). **Z. J. Ding:** Conceptualization (equal); Funding acquisition (equal); Methodology (equal); Project administration (equal); Software (equal); Supervision (equal); Visualization (equal); Writing – review & editing (equal).

DATA AVAILABILITY

The data that support the findings of this study are available from the corresponding authors upon reasonable request.

REFERENCES

[1]J. J. Donovan, J. I. Goldstein, D. E. Newbury, P. Echlin, D. C. Joy, C. Fiori, and E. Lifshin, *Scanning Electron Microscopy and X-ray Microanalysis* (Plenum, 1992).

06 December 2024 01:20:56

© Author(s) 2024

[2]L. Reimer, *Scanning Electron Microscopy: Physics of Image Formation and Microanalysis* (Springer, 1985).
[3]Z. L. Wang, *Reflection Electron Microscopy and Spectroscopy for Surface Analysis* (Cambridge University Press, 1996).
[4]M. Dapor, "Backscattering of low energy electrons from carbon films deposited on aluminum: A Monte Carlo simulation," J. Appl. Phys. **95**, 718–721 (2004).
[5]A. J. Dekker, "Secondary electron emission," Solid State Phys. **6**, 251–311 (1958).
[6]O. C. Wells, "Scanning electron microscopy," in *Encyclopedia of Materials: Science and Technology*, 2nd ed. (Elsevier, Oxford, 2001), pp. 8265–8269.
[7]Y. B. Zou, S. F. Mao, B. Da, and Z. J. Ding, "Surface sensitivity of secondary electrons emitted from amorphous solids: Calculation of mean escape depth by a Monte Carlo method," J. Appl. Phys. **120**, 235102 (2016).
[8]H. Niedrig, "Physical background of electron backscattering," Scanning **1**, 17–34 (1978).
[9]H. Seiler, "Secondary electron emission in the scanning electron microscope," J. Appl. Phys. **54**, R1–R18 (1983).
[10]S. F. Mao, Y. G. Li, R. G. Zeng, and Z. J. Ding, "Electron inelastic scattering and secondary electron emission calculated without the single pole approximation," J. Appl. Phys. **104**, 114907 (2008).
[11]R. Udiljak, D. Anderson, M. Lisak, J. Puech, and V. E. Semenov, "Multipactor in a waveguide iris," IEEE Trans. Plasma. Sci. **35**, 388–395 (2007).
[12]M. Setvín, U. Aschauer, P. Scheiber, Y. F. Li, W. Hou, M. Schmid, A. Selloni, and U. Diebold, "Reaction of O_2 with subsurface oxygen vacancies on TiO_2 anatase (101)," Science **341**, 988–991 (2013).
[13]A. Tomala, A. Karpinska, W. S. M. Werner, A. Olver, and H. Störi, "Tribological properties of additives for water-based lubricants," Wear **269**, 804–810 (2010).
[14]L. Reimer, *Image Formation in Low-Voltage Scanning Electron Microscopy* (SPIE Press, 1993), p. 12.
[15]H. Niedrig, "Electron backscattering from thin films," J. Appl. Phys. **53**, R15–R49 (1982).
[16]L. Reimer, *Transmission Electron Microscopy: Physics of Image Formation and Microanalysis* (Springer, 2013).
[17]H. Kim, T. Negishi, M. Kudo, H. Takei, and K. Yasuda, "Quantitative backscattered electron imaging of field emission scanning electron microscopy for discrimination of nano-scale elements with nm-order spatial resolution," J. Elect. Microsc. **59**, 379–385 (2010).
[18]H. J. Hunger and L. Küchler, "Measurements of the electron backscattering coefficient for quantitative EPMA in the energy range of 4 to 40 keV," Phys. Status Solidi A **56**, K45–K48 (1979).
[19]C. Merlet, "Accurate description of surface ionization in electron probe microanalysis: An improved formulation," X-ray Spectrom. **21**, 229–238 (1992).
[20]E. H. Darlington and V. E. Cosslett, "Backscattering of 0.5–10keV electrons from solid targets," J. Phys. D: Appl. Phys. **5**, 1969 (1972).
[21]D. C. Joy, "A database on electron-solid interactions," Scanning **17**, 270–275 (1995).
[22]F. Akbari, "A comprehensive open-access database of electron backscattering coefficients for energies ranging from 0.1 keV to 15 MeV," Med. Phys. **50**, 5920–5929 (2023).
[23]M. M. El Gomati, C. G. H. Walker, A. M. D. Assa'd, and M. Zadražil, "Theory experiment comparison of the electron backscattering factor from solids at low electron energy (250–5,000 eV)," Scanning **30**, 2–15 (2008).
[24]S. H. Kim, M. G. Pia, T. Basaglia, M. C. Han, G. Hoff, C. H. Kim, and P. Saracco, "Validation test of Geant4 simulation of electron backscattering," IEEE Trans. Nucl. Sci. **62**, 451–479 (2015).
[25]R. Shimizu and Z. J. Ding, "Monte Carlo modelling of electron-solid interactions," Rep. Prog. Phys. **55**, 487 (1992).
[26]D. C. Joy, *Monte Carlo Modeling for Electron Microscopy and Microanalysis* (Oxford University Press, 1995).
[27]M. Dapor, *Transport of Energetic Electrons in Solids: Computer Simulation with Applications to Materials Analysis and Characterization* (Springer, 2023).
[28]Z. J. Ding and R. Shimizu, "A Monte Carlo modeling of electron interaction with solids including cascade secondary electron production," Scanning **18**, 92–113 (1996).
[29]Z. J. Ding, X. D. Tang, and R. Shimizu, "Monte Carlo study of secondary electron emission," J. Appl. Phys. **89**, 718–726 (2001).
[30]Z. J. Ding, H. M. Li, K. Goto, Y. Z. Jiang, and R. Shimizu, "Energy spectra of backscattered electrons in Auger electron spectroscopy: Comparison of Monte Carlo simulations with experiment," J. Appl. Phys. **96**, 4598–4606 (2004).
[31]H. M. Li and Z. J. Ding, "Monte Carlo simulation of secondary electron and backscattered electron images in scanning electron microscopy for specimen with complex geometric structure," Scanning **27**, 254–267 (2005).
[32]Y. T. Yue, H. M. Li, and Z. J. Ding, "Monte Carlo simulation of secondary electron and backscattered electron images for a nanoparticle-matrix system," J. Phys. D: Appl. Phys. **38**, 1966–1977 (2005).
[33]J. S. Villarrubia, N. W. M. Ritchie, and J. R. Lowney, "Monte Carlo modeling of secondary electron imaging in three dimensions," Proc. SPIE **6518**, 65180K (2007).
[34]P. Zhang, H. Y. Wang, Y. G. Li, S. F. Mao, and Z. J. Ding, "Monte Carlo simulation of secondary electron images for real sample structures in scanning electron microscopy," Scanning **34**, 145–150 (2012).
[35]Y. G. Li, P. Zhang, and Z. J. Ding, "Monte Carlo simulation of CD-SEM images for linewidth and critical dimension metrology," Scanning **35**, 127–139 (2013).
[36]Y. B. Zou, M. S. S. Khan, H. M. Li, Y. G. Li, W. Li, S. T. Gao, L. S. Liu, and Z. J. Ding, "Use of model-based library in critical dimension measurement by CD-SEM," Measurement **123**, 150–162 (2018).
[37]A. Hussain, L. Yang, S. Mao, B. Da, K. Tőkési, and Z. J. Ding, "Determination of electron backscattering coefficient of beryllium by a high-precision Monte Carlo simulation," Nucl. Mater. Energy **26**, 100862 (2021).
[38]L. H. Yang, A. Hussain, S. F. Mao, B. Da, K. Tőkési, and Z. J. Ding, "Electron backscattering coefficients of molybdenum and tungsten based on the Monte Carlo simulations," J. Nucl. Mater. **553**, 153042 (2021).
[39]K. Murata, D. F. Kyser, and C. H. Ting, "Monte Carlo simulation of fast secondary electron production in electron beam resists," J. Appl. Phys. **52**, 4396–4405 (1981).
[40]Z. J. Ding and R. Shimizu, "Monte Carlo study of backscattering and secondary electron generation," Surf. Sci. **197**, 539–554 (1988).
[41]M. Dapor, "Monte Carlo simulation of backscattered electrons and energy from thick targets and surface films," Phys. Rev. B **46**, 618 (1992).
[42]J. P. Ganachaud and A. Mokrani, "Theoretical study of the secondary electron emission of insulating targets," Surf. Sci. **334**, 329–341 (1995).
[43]Z. J. Ding, C. Li, B. Da, and J. W. Liu, "Charging effect induced by electron beam irradiation: A review," Sci. Technol. Adv. Mater. **22**, 932–971 (2021).
[44]T. Koshikawa and R. Shimizu, "A Monte Carlo calculation of low-energy secondary electron emission from metals," J. Phys. D: Appl. Phys. **7**, 1303 (1974).
[45]H. J. Fitting and J. Reinhardt, "Monte-Carlo simulation of keV-electron scattering in solid targets," Phys. Status Solidi A **88**, 245–259 (1985).
[46]D. C. Joy, "A model for calculating secondary and backscattered electron yields," J. Microsc. **147**, 51–64 (1987).
[47]J. C. Kuhr and H. J. Fitting, "Monte-Carlo simulation of low energy electron scattering in solids," Phys. Status Solidi A **172**, 433–450 (1999).
[48]D. R. Penn, "Electron mean-free-path calculations using a model dielectric function," Phys. Rev. B **35**, 482 (1987).
[49]H. T. Chen, Y. B. Zou, S. F. Mao, M. S. S. Khan, K. Tokesi, and Z. J. Ding, "Influence of energy loss function to the Monte Carlo simulated electron backscattering coefficient," Sci. Rep. **12**, 18201 (2022).
[50]N. F. Mott, "The scattering of fast electrons by atomic nuclei," Proc. R. Soc. Lond. A **124**, 425–442 (1929).
[51]H. Xu, B. Da, J. Tóth, K. Tőkési, and Z. J. Ding, "Absolute determination of optical constants by reflection electron energy loss spectroscopy," Phys. Rev. B **95**, 195417 (2017).
[52]E. D. Palik, *Handbook of Optical Constants of Solids*, 3rd ed. (Academic Press, 1998).

06 December 2024 01:20:56

© Author(s) 2024

[53]W. S. Werner, K. Glantschnig, and C. Ambrosch-Draxl, "Optical constants and inelastic electron-scattering data for 17 elemental metals," J. Phys. Chem. Ref. Data **38**, 1013–1092 (2009).
[54]F. Salvat, A. Jablonski, and C. J. Powell, "ELSEPA—Dirac partial-wave calculation of elastic scattering of electrons and positrons by atoms, positive ions and molecules," Comput. Phys. Commun. **165**, 157–190 (2005).
[55]J. P. Desclaux, "A multiconfiguration relativistic Dirac-Fock program," Comput. Phys. Commun. **9**, 31–45 (1975).
[56]J. B. Furness and I. E. McCarthy, "Semiphenomenological optical model for electron scattering on atoms," J. Phys. B **6**, 2280 (1973).
[57]F. Salvat, "Optical-model potential for electron and positron elastic scattering by atoms," Phys. Rev. A **68**, 012708 (2003).
[58]P. Nozieres and D. Pines, *The Theory of Quantum Liquids: Superfluid Bose Liquids* (CRC Press, 2018).
[59]S. Tanuma, C. J. Powell, and D. R. Penn, "Use of sum rules on the energy-loss function for the evaluation of experimental optical data," J. Electr. Spectrosc. Relat. Phenom. **62**, 95–109 (1993).
[60]G. D. Mahan, *Many-Particle Physics* (Springer, 2013).
[61]J. Pierron, C. Inguimbert, M. Belhaj, T. Gineste, J. Puech, and M. Raine, "Electron emission yield for low energy electrons: Monte Carlo simulation and experimental comparison for Al, Ag, and Si," J. Appl. Phys. **121**, 215107 (2017).
[62]M. Dapor, "Monte Carlo simulation of secondary electron emission from dielectric targets," J. Phys.: Conf. Ser. **402**, 012003 (2012).
[63]B. Da, H. Shinotsuka, H. Yoshikawa, Z. J. Ding, and S. Tanuma, "Extended Mermin method for calculating the electron inelastic mean free path," Phys. Rev. Lett. **113**, 063201 (2014).
[64]H. Shinotsuka, S. Tanuma, C. J. Powell, and D. R. Penn, "Calculations of electron inelastic mean free paths. X. Data for 41 elemental solids over the 50 eV to 200 keV range with the relativistic full Penn algorithm," Surf. Interface Anal. **47**, 871–888 (2015).
[65]B. Da, X. Liu, L. H. Yang, J. M. Gong, Z. J. Ding, H. Shinotsuka, J. W. Liu, H. Yoshikawa, and S. Tanuma, "Evaluation of dielectric function models for calculation of electron inelastic mean free path," J. Appl. Phys. **131**, 175301 (2022).
[66]E. D. Palik, *Handbook of Optical Constants of Solids* (Academic Press, 1991).
[67]B. L. Henke, E. M. Gullikson, and J. C. Davis, "X-ray interactions: Photoabsorption, scattering, transmission, and reflection at E = 50–30,000 eV, Z = 1–92," At. Data Nucl. Data Tables **54**, 181–342 (1993).
[68]D. E. Cullen, J. H. Hubbell, and L. Kissel, *EPDL97: The Evaluated Photo Data library97 Version* (Lawrence Livermore National Lab, 1997).
[69]L. H. Yang, K. Tőkési, B. Da, and Z. J. Ding, "Determination of electron inelastic mean free path of three transition metals from reflection electron energy loss spectroscopy spectrum measurement data," Eur. Phys. J. D **73**, 1–19 (2019).
[70]S. Tanuma, C. J. Powell, and D. R. Penn, "Calculations of electron inelastic mean free paths. IX. Data for 41 elemental solids over the 50 eV to 30 keV range," Surf. Interface Anal. **43**, 689–713 (2011).
[71]K. F. J. Heinrich, "Electron probe microanalysis by specimen current measurement," in *Proceedings of the 4th International Conference on X-ray Optics and Microanalysis*, edited by R. Castaing, P. Deschamps, and J. Philibert (Hermann, Paris, 1966), p. 159.
[72]H. E. Bishop, "Electron scattering and x-ray production," Ph.D. dissertation (University of Cambridge, 1966).
[73]J. Philibert, and E. Weinryb, "The use of specimen current in electron-probe microanalysis," in *Proceedings of the 3rd International Conference on X-ray Optics and. Microanalysis* (Academic, New York, 1963), p. 163.
[74]L. Reimer and C. Tollkamp, "Measuring the backscattering coefficient and secondary electron yield inside a scanning electron microscope," Scanning **3**, 35–39 (1980).
[75]D. B. Wittry, "Secondary electron emission in the electron probe," in *Proceedings of the 4th International Conference on X-ray Optics and Microanalysis*, edited by R. Castaing, P. Deschamps, and J. Philibert (Hermann, Paris, 1966), pp. 168–180.
[76]M. S. S. Khan, S. F. Mao, Y. B. Zou, D. B. Lu, B. Da, Y. G. Li, and Z. J. Ding, "Extensive theoretical quantification of secondary electron emission from silicon," Vacuum **215**, 112257 (2023).
[77]O. Mansour, A. Kadoun, L. Khouchaf, and C. Mathieu, "Monte Carlo simulation of the electron beam scattering under water vapor environment at low energy," Vacuum **87**, 11–15 (2013).
[78]H. J. Seok, Y. J. Kang, J. Kim, D. H. Kim, S. B. Heo, S. J. Kang, and H. K. Kim, "Tetrahedral amorphous carbon prepared filter cathodic vacuum arc for hole transport layers in perovskite solar cells and quantum dots LEDs," Sci. Technol. Adv. Mater. **20**, 1118–1130 (2019).
[79]L. H. Yang, J. M. Gong, A. Sulyok, M. Menyhárd, G. Sáfrán, K. Tőkési, and Z. J. Ding, "Optical properties of amorphous carbon determined by reflection electron energy loss spectroscopy spectra," Phys. Chem. Chem. Phys. **23**, 25335–25346 (2021).
[80]I. A. Sorokin and N. S. Sergeev, "Measurements of secondary electron emission yield in the linear plasma simulator BPD-PSI," Vacuum **217**, 112528 (2023).

06 December 2024 01:20:56

© Author(s) 2024